Attachment of fiber array adhesive through side contact

Carmel S. Majidi,[a] Richard E. Groff, and Ronald S. Fearing
Department of Electrical Engineering and Computer Science (EECS) University of California, Berkeley, California 94720

(Received 17 March 2005; accepted 30 September 2005; published online 28 November 2005)

Very slender cylindrical fibers are capable of bending over and maintaining side contact with an opposing substrate even as the fibers are pulled away, providing a mode of adhesion for fiber array adhesives. This paper analyzes side contact and its effect on normal adhesion and provides guidelines for fiber length to achieve side contact under zero load as a function of elastic modulus, area moment of inertia, initial geometry, and energy of adhesion between fiber and substrate. Numerical results for several relevant geometries are presented as well as a comparison to recently reported normal adhesion measurements of multiwalled carbon nanotube arrays. © *2005 American Institute of Physics*. [DOI: 10.1063/1.2128697]

I. INTRODUCTION

The dry adhesive systems of geckos and anoles consist of arrays of hierarchically structured hairs called setae. Recent work has identified van der Waals as the primary adhesive forces in these systems.[1,2] Made from keratin, a stiff material (elastic modulus $E \approx 3-15$ GPa), the micro- and nanostructures of the setae create a low effective modulus for the array,[3–5] as well as provide a "self-cleaning" property.[6] These natural adhesive systems have motivated recent papers on analysis and synthesis of fiber array adhesives.[3–5,7–14] From this work emerged perhaps the most important factor for effective adhesion, that each fiber attachment must produce a "long bond."[3,8] This allows for load sharing among multiple fiber attachments without some detaching prematurely during pulloff due to misalignments or surface irregularities. Long bonds can be achieved, for example, by angling the fibers so that they bend in a cantilever mode[7] or by using curved fibers which straighten under tensile load.[3]

The current paper explores another mechanism for achieving long bonds, using simple cylindrical fibers with a very high aspect ratio, for example, the 0.2-μm-diam, 60 μm epoxy fibers in Ref. 8. Under a large enough compressive preload, such a fiber will bend and contact an opposing substrate on its side, as illustrated in Fig. 1, a configuration henceforth referred to as "side contact." Due to surface forces between the fiber and opposing substrate, side contact can be stable even as the fiber is being pulled from the substrate. Indeed, recent measurements of normal adhesion for an array of carbon nanotubes[15] were found to concur with the side contact model's predictions, as discussed in Sec. III. Though fiber array adhesives are bioinspired, the side contact mode of adhesion is distinct from that used by gecko setae, where contact is generally limited to the plate-like spatulae at the tips.

II. ANALYSIS

This section analyzes the behavior of a single slender fiber pushed against an opposing flat substrate. The fiber's loading cycle begins with a preload $P_i > 0$ that pushes the fiber into an opposing flat substrate causing side contact [Fig. 1(c)]. The preload is then relaxed to a continuous load $P < P_i$ [Fig. 1(d)]. If slender enough, a fiber will maintain side contact even when P is negative. The fiber exhibits contact hysteresis analogous to that seen in the Johnson-Kendall-Roberts (JKR) model for adhering elastic spheres.[16] The

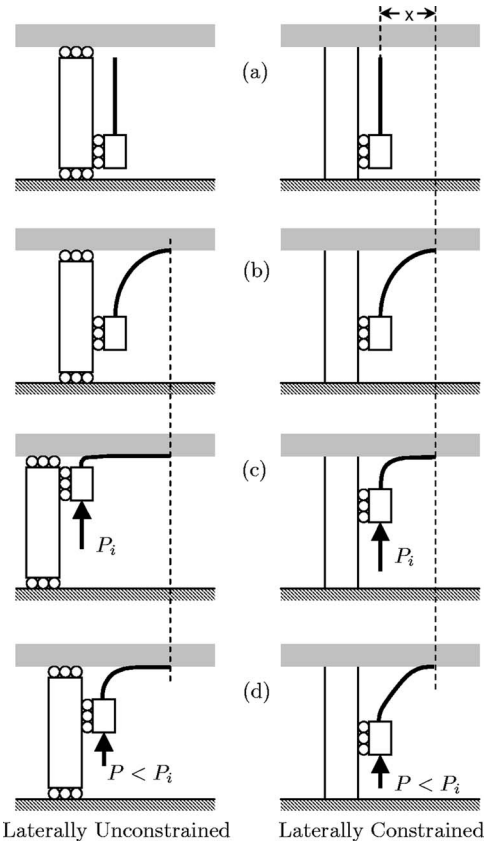

FIG. 1. Loading cycle and qualitative fiber shapes for a fiber completely clamped to a laterally unconstrained and laterally constrained support. (a) Initial configuration. (b) Fiber tip at angle $\pi/2$, side contact begins, tip no longer slides relative to opposing substrate. (c) Maximum value of preload P_i. (d) Preload relaxed to continuous load P, which can be negative.

[a]Electronic mail: cmajidi@eecs.berkeley.edu

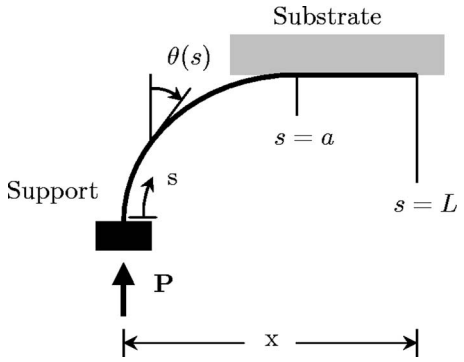

FIG. 2. Deformation of an elastic fiber, completely clamped vertically at its base, making contact with an adhering substrate over a length $L-a$.

analysis predicts contact length between the fiber and the opposing substrate under continuous load P, from which fiber pulloff force can be determined.

The fiber is treated as an elastica of length L, radius R, and elastic modulus E, subject to an external applied load P. Elastica assumes inextensible planar deformation, which was checked to hold for the geometry and loads considered in this paper. The energy method used to determine fiber bending is similar to that used in Ref. 17, which studied the self-adhesion of a folded thin film.

As shown in Fig. 2, the function $\theta(s)$ is defined to be the fiber slope at a distance s along the fiber from its base. Contact is made with an adhering flat along the segment $(a,L]$, while $[0,a]$ is the unattached portion of the fiber.

A. Preload

During preload, we assume that the fiber slips freely along the substrate until interfacial forces cause it to *stick*, preventing further slipping. Let x denote the lateral deflection of the fiber tip (relative to its base) corresponding to when stick first occurs. For example, in the extreme case of no slip, $x=0$, while for frictionless contact, x is undefined. In the current analysis, the fiber tip is assumed to stick when side contact begins, i.e., when $\theta(L)=\pi/2$ [see Fig. 1(b)], since side contact provides increased contact area, which in turn provides increased shear resistance. According to the governing equations for elastica, this configuration corresponds to a lateral tip displacement of $x=2p/k$ where $p=\sin(\pi/4)$, $k=K(p)/L$, and $K(\cdot)$ is the complete elliptic integral of the second kind.[18] Carrying out the computation, it is found that

$$x=[\sqrt{2}/K(1/\sqrt{2})]L=0.763L. \tag{1}$$

As preload continues up to its maximum value P_i, the fiber tip can no longer slide relative to the substrate and the constraints on the support now play an important role. For the laterally unconstrained case (Fig. 1, left), the support will continue to move laterally as the support approaches the substrate. Alternatively, for the laterally constrained case (Fig. 1, right), the lateral displacement between the fiber tip and support remains constant at x as the support approaches the substrate. [Note that the shape of a fiber with a laterally constrained support and frictionless contact with the opposing substrate will be the same as that of a fiber with a laterally unconstrained support and x as defined in (1).] In practice, the array backing is typically free to move laterally in the manner that best accommodates attachment. Due to the mechanical coupling of the fibers through the backing, the lateral movement of individual fiber supports will be restricted, but not necessarily to the extent that the lateral displacement between the tip and support remains constant. The current analysis separately examines constrained and unconstrained supports, with the understanding that the actual behavior of an individual fiber lies somewhere between these two cases.

B. Energy of adhesion per contact length ω

A fiber sticks to an opposing substrate due to surface forces. This interaction is characterized by ω, the energy of adhesion per unit contact length. When a cylinder lies on a flat surface, as analyzed in Refs. 5 and 19, interfacial forces between the fiber and substrate will cause the fiber cross section to deform and make contact over a width $2c$. Assuming linear elasticity, the corresponding strain energy release rate is found to be

$$G=\pi Ec^3/32(1-\nu^2)R^2, \tag{2}$$

where ν is Poisson's ratio for the cylinder. Integrating G to obtain the strain energy and adding the energy of adhesion, the total potential energy per unit length of contact is

$$U(c)=\frac{\pi Ec^4}{128(1-\nu^2)R^2}-W(2c). \tag{3}$$

where W is the work of adhesion between the two surfaces.

For a stable attached equilibrium, $\partial\hat{U}/\partial\hat{c}=0$ and $c>0$, which gives

$$c_{\mathrm{eq}}=2\left[\frac{8W(1-\nu^2)R^2}{\pi E}\right]^{1/3}. \tag{4}$$

The energy of adhesion per unit length for a cylinder in contact with a flat is given by

$$\omega=-U(c_{\mathrm{eq}})=6\left[\frac{(1-\nu^2)R^2W^4}{\pi E}\right]^{1/3}. \tag{5}$$

C. Laterally constrained support

The fiber configuration at equilibrium is the one that minimizes the total potential energy U_{tot}. For the current system, U_{tot} is the sum of the elastic strain energy and the adhesion potential minus the work of the external load,

$$U_{\mathrm{tot}}=\int_0^a\left[\frac{EI}{2}\left(\frac{\partial\theta}{ls}\right)^2+P\cos\theta\right]ds-\omega(L-a), \tag{6}$$

where $I=\pi R^4/4$ is the area moment of inertia. At equilibrium, U_{tot} is minimized with respect to $\theta(s)$ and a, subject to the boundary conditions

$$\theta(0)=0 \text{ and } \theta(a)=\pi/2 \tag{7}$$

and the constraint that the lateral displacement between the support and tip remain fixed, expressed as the isoperimetric condition

$$\int_0^a \sin\theta ds = x - (L-a) = a - \left[1 - \frac{\sqrt{2}}{K(1/\sqrt{2})}\right]L. \tag{8}$$

Employing the method of Lagrangian multipliers,[20] the work to maintain the isoperimetric constraint (8) can be included in the expression for potential energy, yielding

$$U_{\text{tot}} = \int_0^a \left[\frac{EI}{2}\left(\frac{\partial\theta}{ls}\right)^2 + P\cos\theta + \lambda\sin\theta\right]ds - \omega(L-a), \tag{9}$$

where the undetermined multiplier λ is a *constant*. Physically, λ is the lateral force transmitted by the support.

Introducing the nondimensional parameters

$$\hat{s} = \frac{s}{L}, \quad \hat{a} = \frac{a}{L},$$

$$\hat{P} = \frac{PL^2}{EI}, \quad \hat{\lambda} = \frac{\lambda L^2}{EI},$$

$$\hat{\omega} = \frac{\omega L^2}{EI}, \quad \hat{U}_{\text{tot}} = \frac{U_{\text{tot}}L}{EI}, \tag{10}$$

$$\hat{x} = \frac{x}{L},$$

Eq. (9) can be rewritten as

$$\hat{U}_{\text{tot}} = \int_0^{\hat{a}} \left[\frac{1}{2}\left(\frac{\partial\theta}{\partial\hat{s}}\right)^2 + \hat{P}\cos\theta + \hat{\lambda}\sin\theta\right]d\hat{s} - \hat{\omega}(1-\hat{a}). \tag{11}$$

Similarly, (8) becomes

$$\int_0^{\hat{a}} \sin\theta d\hat{s} = \hat{a} - \left[1 - \frac{\sqrt{2}}{K(1/\sqrt{2})}\right]. \tag{12}$$

To minimize (11) with respect to the function $\theta(\hat{s})$ it is necessary only to minimize the integral term. Thus $\theta(\hat{s})$ must satisfy the Euler-Lagrange equation,[20]

$$\frac{\partial^2\theta}{\partial\hat{s}^2} = -\hat{P}\sin\theta + \hat{\lambda}\cos\theta. \tag{13}$$

This ordinary differential equation (ODE) with boundary conditions given by (7) is solved numerically to determine $\theta = \theta(\hat{s}, \hat{a}, \hat{\lambda})$. Next, the isoperimetric condition (12) is used to eliminate $\hat{\lambda}$, resulting in an expression $\theta = \theta(\hat{s}, \hat{a})$. Lastly, the value of $\hat{a}$ at equilibrium is defined as $\hat{a}_{\text{eq}} = \{\hat{a} \in [0,1] : \partial\hat{U}_{\text{tot}}/\partial\hat{a} = 0\}$. The fiber shape at equilibrium is defined by $\theta_{\text{eq}} = \theta(\hat{s}, \hat{a}_{\text{eq}})$.

D. Laterally unconstrained support

The analysis for the laterally unconstrained support proceeds similarly, minimizing potential energy (6) subject to boundary conditions (7), but in this case the isoperimetric condition (8) is dropped. Thus, $\theta(\hat{s}, \hat{a})$ must satisfy the Euler-Lagrange equation,

$$\frac{\partial^2\theta}{\partial\hat{s}^2} = -\hat{P}\sin\theta, \tag{14}$$

for the boundary conditions (7). As before, $\hat{a}$ at equilibrium is $\hat{a}_{\text{eq}} = \{\hat{a} \in [0,1] : \partial\hat{U}_{\text{tot}}/\partial\hat{a} = 0\}$, where now

$$\hat{U}_{\text{tot}} = \int_0^{\hat{a}} \left[\frac{1}{2}\left(\frac{\partial\theta}{\partial\hat{s}}\right)^2 + \hat{P}\cos\theta\right]d\hat{s} - \hat{\omega}(1-\hat{a}). \tag{15}$$

The fiber shape at equilibrium is defined by $\theta_{\text{eq}} = \theta(\hat{s}, \hat{a}_{\text{eq}})$.

If no external applied load acts on the system, then closed form solutions for $\theta_{\text{eq}}(\hat{s})$ and $\hat{a}_{\text{eq}}$ can be obtained. Solving (14) for $\hat{P} = 0$, the fiber is found to form a circular arc of radius $\hat{a}/(\pi/2)$. Hence,

$$\hat{U}_{\text{tot}}|_{\hat{P}=0} = (\pi/2)^2/2\hat{a} - \hat{\omega}(1-\hat{a}). \tag{16}$$

At equilibrium, $\partial\hat{U}_{\text{tot}}/\partial\hat{a} = 0$, which implies that $\hat{a}_{\text{eq}} = (\pi/2)/\sqrt{2\hat{\omega}}$. It is important to note that this value is independent of the total length of the fiber but only holds if $L > a_{\text{eq}}$. Hence, for the laterally unconstrained support, finite side contact under zero applied load is only possible when the fiber length exceeds the critical value

$$L_{\text{cr}} = \frac{\pi}{2}\sqrt{\frac{EI}{2\omega}}. \tag{17}$$

E. Numerical solution

The relationship between the nondimensional external applied load $\hat{P}$ and the nondimensional contact length $1-\hat{a}$ was numerically computed for fibers with laterally constrained as well as laterally unconstrained support. The steps for solving the constrained case will be described here. The simpler unconstrained case follows an analogous procedure.

The nondimensional contact length $1-\hat{a}$ resulting from a nondimensional external applied load $\hat{P}$ is determined by finding $\hat{a}$, $\theta(\hat{s})$, and $\hat{\lambda}$ that minimize $\hat{U}_{\text{tot}}$ while satisfying the isoperimetric condition and boundary conditions. Given values of $\hat{a}$ and $\hat{\lambda}$, a boundary-value problem (BVP) solver can be used to find $\theta(\hat{s}, \hat{a}, \hat{\lambda})$ that satisfies the ODE (13) and boundary conditions (7) given in Sec. II C. Then a zero finder can be applied in conjunction with the BVP solver to find $\hat{\lambda}^*(\hat{a})$ such that $\theta[\hat{s}, \hat{a}, \hat{\lambda}^*(\hat{a})]$ satisfies the isoperimetric constraint (12). Now $\hat{U}_{\text{tot}}$ (9) can be written as a function of just $\hat{a}$, and plotting $\hat{U}_{\text{tot}}$ vs $\hat{a}$ reveals a convex dependency. Numerical minimization is used to find $\hat{a}_{\text{eq}}$, the value of $\hat{a}$ that minimizes $\hat{U}_{\text{tot}}$. Thus a nondimensional external applied load $\hat{P}$ results in a nondimensional contact length $1-\hat{a}_{\text{eq}}$. In addition, the equilibrium position of the fiber under nondimensional external applied load $\hat{P}$ is given by $\theta_{\text{eq}}(\hat{s}) = \theta[\hat{s}, \hat{a}_{\text{eq}}, \hat{\lambda}^*(\hat{a}_{\text{eq}})]$. All of the above tasks were implemented in MATLAB6.5 (The Mathworks, Inc., 2002) using built-in functions available in the optimization and BVP solver toolboxes.

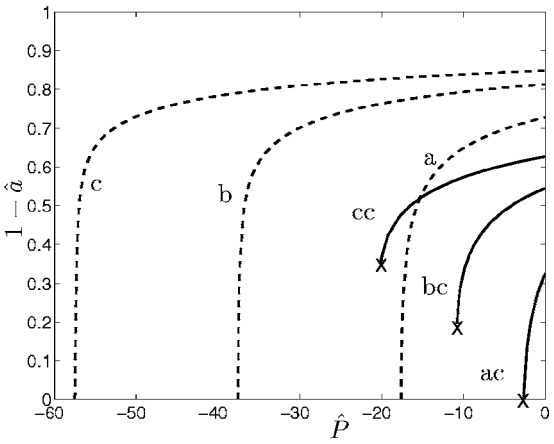

FIG. 3. Dependency of nondimensional contact length $1-\hat{a}$ on applied load parameter $\hat{P}=PL^2/EI$; curves *a*, *b*, and *c* correspond to a laterally unconstrained support with $\hat{\omega}=16.7$, 35.4, and 54.1, respectively; curves *ac*, *bc*, and *cc* correspond to a laterally constrained support with $\hat{\omega}=16.7$, 35.4, and 54.1, respectively. The × denotes spontaneous detachment.

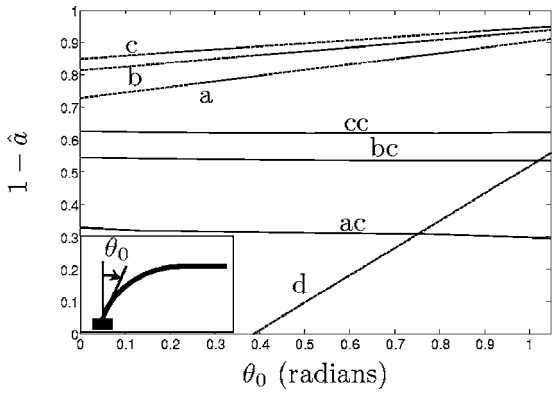

FIG. 4. Dependency of nondimensional contact length $1-\hat{a}$ on inclined fiber slope θ_0 for zero applied load. The curve labels are the same as for Fig. 3, with the addition of curve *d*, which corresponds to a laterally unconstrained support with $\hat{\omega}=0.7$.

III. DISCUSSION

Figure 3 shows the dependence of nondimensional contact length on the applied load parameter for both unconstrained and constrained fiber supports. Curves are plotted for three representative values of the nondimensional adhesion parameter $\hat{\omega}$: 16.7, 35.4, and 54.1. The first two values were specifically chosen to correspond to the epoxy fibers of Ref. 8 and the multiwalled carbon nanotube (MWCNT) fibers of Ref. 15, respectively.

The results in Fig. 3 clearly show that finite contact length is possible even for $\hat{P}<0$ when $\hat{\omega}$ is sufficiently large. For such systems, the dependency of contact length on applied load is analogous to that of contact area on applied load for the sphere-flat model studied in the JKR theory. In particular, in the case that the support is laterally constrained, there is a distinct maximum pulloff load, above which stable contact is no longer possible (indicated by × in the figure).

A. Inclined fibers

The analysis in the previous section presented only vertical fibers, but inclined fibers are known to be important for other modes of fiber array adhesion.[5,7] The boundary conditions in the analysis may be altered to allow for fibers initially inclined at θ_0, i.e., $\theta(0)=\theta_0$. For the laterally constrained support, inclining the fiber also changes the lateral displacement at which side contact begins, *x*, which appears in the isoperimetric constraint (8). For the unconstrained support, a closed form solution can be found for nondimensional contact length under zero applied load as a function of angle at the base, specifically

$$1-\hat{a}=1-(\pi/2-\theta_0)/\sqrt{2\hat{\omega}}. \tag{18}$$

The dependency of the nondimensional contact length $1-\hat{a}$ on θ_0 under zero applied load is plotted in Fig. 4 for both constrained and unconstrained supports. Contact length is significantly influenced by incline angle only when $\hat{\omega}$ is small (e.g., $\hat{\omega}=0.7$). Moreover, as illustrated by curve *d* in the figure, side contact for such fibers under zero load requires an incline angle $\theta_0>0$. Rewriting (18), a fiber with laterally unconstrained support and incline θ_0 can make finite side contact under zero applied load only if its length exceed the critical length,

$$L_{\mathrm{cr}}=\left(\frac{\pi}{2}-\theta_0\right)\sqrt{\frac{EI}{2\omega}}. \tag{19}$$

B. Shear resistance

In motivating the isoperimetric constraint for the case of a laterally constrained support it was assumed that the frictional forces associated with side contact were great enough to prevent further horizontal translation of the fiber tip. Such an assumption follows from the notion that the interfacial shear resistance to sliding is linear with the real area of contact,[21–23]

$$F_s=\tau_0 A_r. \tag{20}$$

One approximation for τ_0 may be inferred from the interfacial shear strength corresponding to pulling a carbon nanotube out of a polymer matrix, found to be on the order of 100 MPa.[24] Side contact increases the contact area, given by contact length times contact width, $2(L-a)c_{\mathrm{eq}}$, where c_{eq} is given by (4). One attractive outcome is the possibility that side contact may provide friction enhancement. Indeed, shear strength predictions following from (20) are extremely high. Of course, another mode such as shear peeling may be a more likely cause of shear failure, and so further investigation is required to predict the shear strength of an array of fibers in side contact.

IV. APPLICATION TO MWCNT ARRAYS

The predictions of the current model compare favorably with force measurements collected from an array of carbon nanotubes that have been recently studied.[15] Such an array consists of MWCNTs of length $L=5$ μm and radius $R=7.5$ nm with an array density of 3×10^{10} tubes/cm^2. Previous experiments have shown that the energy of adhesion per unit area for a MWCNT adsorbed on a glass substrate is approximately 330 mJ/m^2.[25] The radial modulus of an

MWCNT is about $E_r=30$ GPa,[26] while the elastic modulus in the axial direction is known to be much larger and here assumed to be $E_a=800$ GPa. Lastly, a Poisson's ratio of $\nu=0.3$ is assumed.

Following from (5), the energy of adhesion per unit length of contact for a MWCNT is $\omega=2.8$ nJ/m, where the radial modulus E_r is used in place of E. Hence, $\hat{\omega}=\omega L^2/E_aI=35.4$. As seen from Fig. 3, this corresponds to a nondimensional applied load that can grow to be as large as 10.8. Multiplying this value by EI/L^2 gives the absolute tensile strength of a single fiber contact, 0.86 nN. Through preliminary testing, Ref. 15 has observed a pulloff force of 4.8 N/cm^2, which suggests an average peel strength of 0.16 nN/tube. One explanation for why this value is smaller than theoretically predicted is that not all MWCNTs are likely to experience their maximum allowable tensile load simultaneously during array detachment. Another possible reason has to do with cross-sectional stiffening caused by residual stresses in the walls of the MWCNTs. In the case of single-walled carbon nanotubes (SWCNTs), it has been demonstrated by Tang *et al.* that residual stresses restrict elastic deformation of the cross section,[27] limiting contact area under surface forces. As a result, the adhesion $\hat{\omega}$ of a nanotube structure is expected to be less than that predicted in (5) for a solid cylinder, leading to a peel strength that may be closer to the experimental value.

V. CONCLUDING REMARKS

Adhesion through side contact is one possible mechanism in which a fiber array adhesive can achieve load sharing among its many contacts, enabling a large overall bond strength. It follows from Sec. III A that side contact can be achieved under zero load if $L>L_{cr}$. Hence, side contact can be obtained with a long length, a low flexural rigidity, a large energy of adhesion, or a large initial incline. Previous studies, however, have shown that the first three properties promote clumping between adjacent fibers,[5,7,12] while the last reduces the clearance between the array backing and substrate and thus limits the ability to accommodate large surface asperities.

The models for constrained and unconstrained supports place bounds on the performance of individual fibers. Fibers with unconstrained support perform better in terms of normal adhesion, but constraints on the fiber support will arise in a fiber array due to mechanical coupling through the array backing. Thus, this analysis provides some insight into the importance of compliance in the array backing in order to decrease mechanical coupling between fibers. As a biological example, the gecko's lamellae, analogous to the array backing, is a thin clothlike flap of skin that appears to provide good compliance between individual setae.

Based on geometry and approximate surface energies, a number of known working fiber adhesives would be predicted to use side contact, including the MWCNT of Ref. 15, the epoxy fibers of Ref. 8, and the silicon nanowires of Ref. 28. Moreover, it was shown that the side contact mechanism described here predicts bounds on the detachment forces that are consistent with measurements on a MWCNT array. This correlation has been accomplished without fitting parameters but provides only a rough estimate of performance. Future work will include study of the shear adhesion of the MWCNT. Future work should also explore the effects of clumping[5,12] or entanglement on adhesion in order to obtain more accurate predictions.

ACKNOWLEDGMENTS

The authors wish to thank Tao Tong and Yang Zhao for discussions of the MWCNT adhesive system and a reviewer for insightful comments. This work was supported by a DCI Postdoctoral Fellowship (R.E.G), DARPA, and NSF NIRT. This material is based upon the work supported by the National Science Foundation under Grant No. EEC-0304730. Any opinions, findings and conclusions, or recommendations expressed in this material are those of the authors and do not necessarily reflect the views of the National Science Foundation (NSF).

[1] K. Autumn, Y. A. Liang, S. T. Hsieh, W. Zesch, W. P. Chan, T. W. Kenny, R. Fearing, and R. J. Full, Nature (London) **405**, 681 (2000).
[2] K. Autumn *et al.*, Proc. Natl. Acad. Sci. U.S.A. **99**, 12252 (2002).
[3] B. N. J. Persson, J. Chem. Phys. **118**, 7614 (2003).
[4] A. Jagota and S. J. Bennison, Integr. Comp. Biol. **42**, 1140 (2002).
[5] N. J. Glassmaker, A. Jagota, C.-Y. Hui, and J. Kim, J. R. Soc., Interface **1**, 1 (2004).
[6] W. R. Hansen and K. Autumn, Proc. Natl. Acad. Sci. U.S.A. **102**, 385 (2005).
[7] M. Sitti and R. S. Fearing, J. Adhes. Sci. Technol. **18**, 1055 (2003).
[8] D. Campolo, S. Jones, and R. S. Fearing, Proceedings of the Third IEEE Conference of Nanotechnology, San Francisco, CA, 2003 (IEEE, New York, 2003), Vol. 2, pp. 856–859.
[9] A. K. Geim, S. V. Dubunos, I. V. Grigorieva, K. S. Novoselov, A. A. Zhukov, and Y. U. Shapoval, Nat. Mater. **2**, 461 (2003).
[10] B. N. J. Persson and S. Gorb, J. Chem. Phys. **119**, 11437 (2003).
[11] C.-Y. Hui, N. J. Glassmaker, T. Tang, and A. Jagota, J. R. Soc., Interface **1**, 35 (2004).
[12] C. Majidi, R. Groff, and R. Fearing, Proceedings of the International Mechanical Engineering Congress and Exposition, Anaheim, CA, 2004 (ASME, New Jersey, 2004).
[13] H. Gao, X. Wang, H. Yao, S. Gorb, and E. Arzt, Mech. Mater. **37**, 275 (2005).
[14] R. Spolenak, S. Gorb, H. Gao, and E. Arzt, Proc. R. Soc. London, Ser. A **461**, 305 (2005).
[15] T. Tong, Y. Zhao, L. Delzet, A. Kashani, and A. Majumdar, presented at the ASME Third Integrated Nanosystems, Design Synthesis and Applications Conference, Pasadena, CA, 2004 (ASME, New Jersey, 2004).
[16] K. L. Johnson, K. Kendall, and J. Roberts, Proc. R. Soc. London, Ser. A **324**, 301 (1971).
[17] N. J. Glassmaker and C. Y. Hui, J. Appl. Phys. **96**, 3429 (2004).
[18] S. P. Timoshenko and J. M. Gere, *Theory of Elastic Stability* (McGraw-Hill, New York, 1961), pp. 76–82.
[19] M. K. Manoj, T. Weaver, C. Y. Hui, and E. J. Kramer, J. Appl. Phys. **80**, 30 (1996).
[20] C. Lanczos, *The Variational Principles of Mechanics*, 4th ed. (Dover, New York, 1970), pp. 59–60.
[21] A. H. Homola, J. N. Israelachvili, P. M. Mcguiggan, and M. L. Gee, Wear **136**, 65 (1990).
[22] E. Rabinowicz, *Friction and Wear of Materials*, 2nd ed. (Wiley, New York, 1995), Chap. 4.
[23] R. W. Carpick, N. Agrait, D. F. Ogletree, and M. Salmeron, J. Vac. Sci. Technol. B **14**, 1289 (1996).
[24] K.-T. Hsiao, J. Alms, and S. Advani, Nanotechnology **14**, 791 (2003).
[25] M. F. Yu, T. Kowalewski, and R. S. Ruoff, Phys. Rev. Lett. **86**, 87 (2001).
[26] I. Palaci, S. Fedrigo, H. Brune, C. Klinke, M. Chen, and E. Riedo, Phys. Rev. Lett. **94**, 175502 (2005).
[27] T. Tang, A. Jagota, and C. Y. Hui, J. Appl. Phys. **97**, 074304 (2005).
[28] R. Dubrow, U.S. Patent No. US2004/0250950 A1 (16 December 2004).